ASSESSMENT OF THE RADIOMETRIC ACCURACY IN A TARGETLESS WORKFLOW USING PIX4D SOFTWARE

M. Cubero-Castan, K. Schneider-Zapp, M. Bellomo, D. Shi, M. Rehak and C. Strecha

Pix4D SA, EPFL Innovation Park - Building F, 1015 Lausanne, Switzerland

ABSTRACT

To compute reflectance from images taken by multispectral sensors aboard UAVs, most users perform radiometric calibration using a target with known reflectance. This workflow is error-prone and not practical for large data acquisitions. With recent advances in multispectral cameras, sensors which measure the sky down-welling irradiance have become available. This enables radiometric calibration without using a target. In this paper, we assess the radiometric accuracy of targetless acquisition using a Sequoia+ camera[1] for both at-ground and in-flight measurements. Most of the measured control points exhibit a high correlation with $R^2 \approx 0.96$ in the computed reflectance factor.

Index Terms— UAVs, targetless workflow, radiometric calibration, multispectral cameras, Pix4D, Sequoia+ camera

1. INTRODUCTION

For several decades, remote sensing has been a useful tool in an increasing range of applications, from broad science disciplines (oceanography, astronomy) to very dedicated applications (mineral spectroscopy, precision agriculture) [1]. The available sensing platforms have evolved, with an increased interest in unmanned aerial vehicles (UAVs) in recent years. For each platform, dedicated multispectral and hyperspectral cameras have been designed to retrieve the reflectance factor of ground materials in several spectral bands. Radiometric accuracy is of prime importance for accurate results. Artifacts due to incorrect radiometry can lead to misinterpretation.

For most spectral cameras, the irradiance reflected by materials at ground is measured. A procedure called radiometric calibration is then needed to compute the reflectance, estimating the sky down-welling irradiance to invert it into the measured reflected irradiance [2]. Different methods for radiometric calibration exist.

The first approach consists of computing the sky down-welling irradiance from measured atmospheric parameters with dedicated softwares like MODTRAN or ATCOR-4 [3]. This traditional method from satellite and aircraft data acquisition is not readily applicable to drone-based data due to different spatial scales, illumination conditions (satellites only yield data without cloud cover), and instrument constraints. Furthermore, the need for accurate parameters to model the atmosphere limits greatly its usage for processing small flights.

A second approach known as target workflow consists of computing the reflectance factor using one or multiple targets with known reflectance. A calibration frame, i.e. a capture of the target with the same illumination condition, is taken before, during or after the flight. Most researchers then use the empirical line method to calibrate their sensors [4, 5]. Several limitations come with this workflow. Firstly, the target should be Lambertian, and if otherwise, the angular distribution of the reflectance should be known, whose measurement is complex [6]. Secondly, the target should be clean and scratchless. Special care should be taken to ensure that its reflectance remains constant throughout the flight time, otherwise, it should be measured repeatedly. Thirdly, since illumination conditions can change rapidly under cloud coverage, calibration frames are required for every change. A simple workflow that can considerably reduce human intervention is required. The aforementioned limitations make this workflow impractical for frequent measurements or large-scale applications such as precision agriculture.

In the case of spaceborne and airborne data, the atmosphere has a non-negligible influence. Due to the low altitude at which UAVs operate, the down-welling irradiance reaching the UAV is practically identical to the one on the ground [3]. Therefore, UAVs can measure the sky down-welling irradiance directly on the platform and thus a compensation for the atmospheric effects is not necessary. Multispectral cameras with sensors that capture this irradiance have recently become available commercially. These sensors can be used to derive reflectance factors with a targetless workflow that does not require an empirical calibration procedure for every acquisition. However, this approach also introduces challenges which need to be tackled, such as properly modelling illumination changes or avoiding sun angle artifacts [7].

In this paper, the radiometric accuracy of a targetless workflow is assessed, using the multispectral camera Sequoia+ mounted on an eBee[2] for flight acquisition, with the

[1] https://www.parrot.com/business-solutions-us/parrot-professional/parrot-sequoia

[2] https://www.sensefly.com/drone/ebee-mapping-drone/

Band name	Wavelength (nm)	FWHM (nm)
Green	550	40
Red	660	40
Red edge	735	10
NIR	790	40

Table 1. Details of Sequoia+ bands.

state-of-the-art of photogrammetric image processing delivered by Pix4D[3]. Both at-ground and in-flight data are analysed. All the processing pipelines presented and assessed in this study are available in Pix4Dmapper starting from version 4.3.

2. MATERIALS AND METHODS

Two data acquisitions were done in order to assess the radiometric quality of the computed reflectance factor in a targetless workflow: a ground measurement to validate the camera and a UAV flight to validate the targetless workflow on a real use case, both for reflectance factors and a vegetation index (Normalized Differences Vegetation Index, or NDVI).

2.1. Data acquisition

The acquisitions were performed with the multispectral camera Sequoia+ designed by Parrot SA, which is composed of 4 monochrome cameras with different narrow-band filters in the visible and near infrared (NIR) domain. The spectral characterization (average wavelength and Full Width Half Maximum, or FWHM) of the cameras is shown in table 1. The camera comes with a "sunshine sensor" which measures the sky down-welling irradiance. It is composed of 4 photodiodes with spectral filters, acquiring the sky irradiance at the same spectral bands as the camera. Reflectance targets were used to assess the camera. Their true reflectance factor was measured with a spectro-radiometer (Flame-S-VIS-NIR, Ocean Optics, USA)[4] using Spectralon^{TM}(LabSphere, USA)[5] as reference. The spectro-radiometer measures irradiance on $2048\,\text{pixels}$ in the visible and NIR spectral range ($350\,\text{nm}$-$1000\,\text{nm}$) with a resolution of $1.5\,\text{nm}$.

2.1.1. Ground validation

A validation measurement was performed to verify the precision and accuracy of the camera/sunshine sensor. With this measurement, we assessed the quality of the retrieved reflectance factor as well as the linearity with respect to exposure time and irradiance. A target composed of 42 different grey patches (6 rows by 7 columns) was observed by the multispectral camera. The camera was mounted on a tripod, viewing the target at nadir. The sunshine sensor was located directly beside the target to measure the same sky down-welling irradiance that is received by the target and avoid effects due to different sun angles. A visualization of the set-up is shown in fig. 1 (a). The reflectance factors of each patch were then computed. The acquisition location was an open space at EPFL, Lausanne, Switzerland ($46°31'6.2''$ N, $6°33'59.4''$ E), which was flat and without any 3D structures close by, in order to prevent reflected light from adjacent objects. The true reflectance factors were measured with the spectro-radiometer.

(a) Validation set-up (b) Example of acquired frame.

Fig. 1. Visualization of the verification set-up. Sequoia+ is mounted on a tripod, looking at the multigray target.

2.1.2. Flight measurement

The flight acquisition was performed using a fixed-wing eBee, manufactured by senseFly SA. The flight area was located close to Vufflens-la-Ville, Switzerland ($46°34'9''$ N, $6°32'29''$ E). 131 frames were acquired for each band, with an overlap of $80\,\%$, resulting in a ground sampling distance (GSD) of $8.25\,\text{cm}$. Ground-truth measurements were performed to geo-reference the project and assess the radiometric accuracy. The acquisition was done with clear sky during the flight and most of the ground-truth measurement with a few cumulus clouds forming at the end of the ground measurements.

Several Ground Control Points (GCPs) were dispatched across the scene to insure good geo-referencing of the project. Their locations were measured using a Real-Time Kinematic (RTK) GPS (Triumph-LS, JAVAD, Russia). They need to be distinguished from radiometric control points (RCPs), which are points whose true reflectance factor was measured with the spectro-radiometer.

To assess the radiometric accuracy of the camera in-flight, three polyester fabric calibration tarps (Group VIII Technologies[6]) of $1.2\,\text{m} \times 1.2\,\text{m}$ were put on the ground, large enough to be seen in-flight. Their edges were measured by the same RTK GPS and added to the GCPs. A good coverage of measured reflectance was provided with reflectance factors of around $34\,\%$, $16\,\%$, and $6.5\,\%$, respectively. Their reflectance factors were measured with the spectro-radiometer. In addition, several natural surfaces (mostly vegetation and soil)

[3]https://pix4d.com/product/pix4dmapper-photogrammetry-software/
[4]https://oceanoptics.com/product/flame-spectrometer/
[5]https://www.labsphere.com/
[6]http://www.group8tech.com/

were measured with the spectro-radiometer thrice to eliminate measurements that were acquired with changing lighting conditions, and geo-referenced, in order to obtain ground-truth for different objects. For each spectro-radiometer measurement, the mean of 50 scans was used. The footprint of the probe corresponded to an area of 1 GSD. During the acquisition, the probe was moved slightly to capture most of the material spectral heterogeneity and obtain an effective footprint corresponding to around 2 to 3 GSD. The accuracy of the absolute location of the measured area was estimated up to 30 cm due to slight variations between the RTK location and the field of view of the probe.

2.2. Processing

Photogrammetric and radiometric image processing were performed with Pix4Dmapper 4.3, in a 3 step workflow which is described below:

- Initial processing: it consisted of estimating the orientation of all images with advanced bundle block adjustment. The scene was geo-referenced using GCPs.
- Dense Point Cloud and DSM: After initial processing, a dense point cloud was generated, from which a Digital Surface Model (DSM) was computed. After initial processing, a 3D mesh was computed, based on the generated point cloud.
- Orthomosaic and Index: Based on the DSM, the points were then radiometrically corrected. Three different orthomaps can be produced: the DSM itself, the reflectance and the index maps. In our study, only reflectance and index maps were assessed.

The RayCloud™, used to assess visually the quality of the reconstruction, is represented in fig. 2. Geometric and RCPs are shown as green and blue nails. The position and orientation of the image captures are shown as green pyramids. The blue dots represent the GPS derived position of the cameras.

Further evaluation steps and plotting have been done with Python (version 2.7). For each RCP, the corresponding pixel was located in the reflectance map. For tarps, the center point was computed from the corners. An area of 2 pixels (16.5 cm) around that point was averaged to account for the spatial referencing accuracy and material heterogeneity. For each band, the spectro-radiometer data was averaged with the known Gaussian spectral sensitivity of the respective band to compute the true values.

3. RESULTS AND DISCUSSION

3.1. Ground validation

Reflectance factors were computed for all exposure times used in the flight acquisition, in order to check the camera

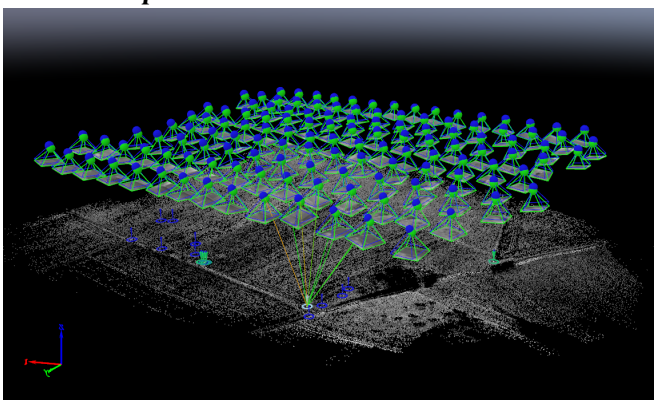

Fig. 2. Visualization of flight acquisition with Pix4D RayCloud™.

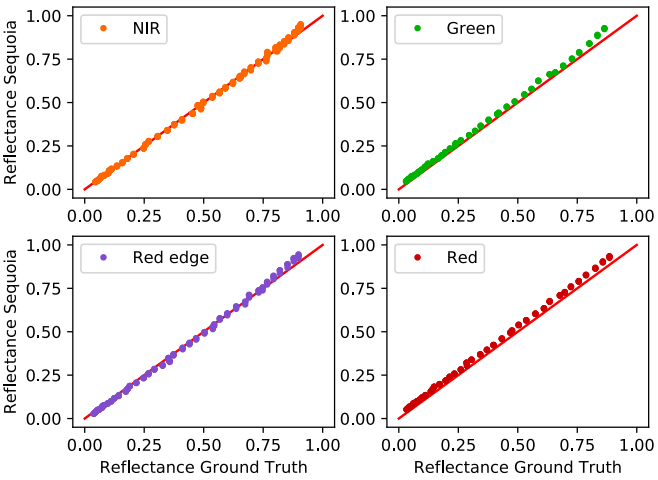

Fig. 3. Comparison of Sequoia+ derived reflectance factors with spectro-radiometer derived ground truth.

behaviour in typical conditions. None of the 42 patches were saturated, allowing to assess the whole range from 2 % to 90 % in reflectance factor. A comparison of the computed reflectance factors with the spectro-radiometer derived ground truth values is shown in fig. 3. The continuous gray line represents the ideal 1:1 case. In general, the estimated values agree well with the ground truth. All bands are very close to the ideal response with approximately 2.5 % Root Mean Square Error (RMSE). For high reflectance factors above 75 %, the discrepancy is higher, with Sequoia+ overestimating the reflectance by approximately 8 %. However natural materials don't exhibit such high reflectance, therefore this limitation does not affect the radiometric quality for typical use cases.

3.2. Flight validation

The ground reference consisted of 7 natural RCPs (vegetation and soil), 3 asphalt road and the 3 fabric targets. Ground truth measured by the spectro-radiometer was compared to

reflectance maps computed with Pix4Dmapper. Only the fabric target with highest reflectance ($34\,\%$) was saturated in the green and red bands. In auto-exposure mode, the camera sets the exposure time that best represents most of the signal. For our scene, most of the materials had a reflectance in green and red bands between $1\,\%$ and $25\,\%$.

Geometrically, the reprojection error was $0.2\,\mathrm{pixel}$, leading to an error of $1.7\,\mathrm{cm}$. The GPS-based geo-referencing showed a shift of $75\,\mathrm{cm}$ horizontally and $240\,\mathrm{cm}$ vertically. This is the expected accuracy for the combination eBee/Sequoia+ without RTK. After the geo-referencing with the GCPs, this shift was reduced to $3.4\,\mathrm{cm}$ horizontally and $5.2\,\mathrm{cm}$ vertically, which is below the GSD of $8.25\,\mathrm{cm}$.

A close match was observed with the ground truth for most of the RCPs. A strong bias (approximately $10\,\%$) has been found for road measurements. This bias might come from differences in lighting conditions between the flight (clear sky) and spectro-radiometer measurements (sun covered by scattered clouds). As roads are materials with high directional reflectance properties, the reflectance is expected to be different in the two lighting conditions. Doing the comparison based only on soil, vegetation and target GCPs, a high correlation between ground truth and computed reflectance is observed, with a coefficient of determination $R^2 \approx 0.96$ for all bands.

The results for the NDVI accuracy is shown in fig. 4. The NDVI reference was computed from the spectro-radiometer derived reflectance factors for the red and NIR bands. The grey continuous line represents the ideal 1:1 case. The four classes of materials are well separated between vegetation and non-vegetation materials by the NDVI. Apart from man-made materials whose NDVI is overestimated, the NDVI of other materials are well retrieved, with RMSE of $3.5\,\%$, and again a high R^2 of about 0.97 for NDVI.

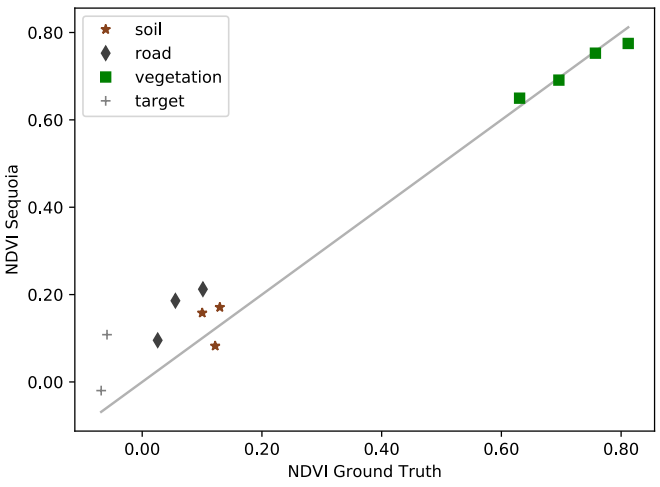

Fig. 4. Comparison between NDVI computed from spectro-radiometer and reconstructed reflectance maps.

4. CONCLUSIONS

With an embedded sunshine sensor, several multispectral cameras enable data acquisition in a targetless workflow, meaning without taking a calibration frame before and/or after the flight. This paper aims to assess the radiometric accuracy in such a workflow for reflectance maps computed by Pix4Dmapper. The camera used for this study is the Sequoia+, manufactured by Parrot SA.

Based on this study, we can conclude that accurate reflectance factors can be computed in a targetless workflow using Pix4Dmapper. A high correlation between ground truth and computed reflectance was observed, with $R^2 \approx 0.96$ for all bands.

References

[1] T. Adão, J. Hruška, L. Pádua, J. Bessa, E. Peres, R. Morais, and J. J. Sousa, "Hyperspectral imaging: A review on UAV-based sensors, data processing and applications for agriculture and forestry," *Remote Sensing*, vol. 9, no. 11, pp. 1110, 2017.

[2] L. Markelin, *Radiometric calibration, validation and correction of multispectral photogrammetric imagery*, Ph.D. thesis, Aalto University School of Engineering, Espoo, Finland, 2013.

[3] D. Schläpfer and J. Nieke, "Operational simulation of at sensor radiance sensitivity using the MODO/MODTRAN4 environment," in *Proceedings EARSeL Fourth Workshop on Imaging Spectroscopy, Warsaw, Poland*, 2005, pp. 611–619.

[4] S. Jakob, R. Zimmermann, and R. Gloaguen, "The need for accurate geometric and radiometric corrections of drone-borne hyperspectral data for mineral exploration: Mephystoa toolbox for pre-processing drone-borne hyperspectral data," *Remote Sensing*, vol. 9, no. 1, 2017.

[5] C. Wang and S. W. Myint, "A simplified empirical line method of radiometric calibration for small unmanned aircraft systems-based remote sensing," *IEEE Journal of Selected Topics in Applied Earth Observations and Remote Sensing*, vol. 8, no. 5, pp. 1876–1885, May 2015.

[6] C. Bruegge, N. Chrien, and D. Haner, "A spectralon BRF data base for MISR calibration applications," *Remote Sensing of Environment*, vol. 76, pp. 354–366, 2001.

[7] E. Honkavaara, L. Markelin, T. Rosnell, and K. Nurminen, "Influence of solar elevation in radiometric and geometric performance of multispectral photogrammetry," *ISPRS Journal of Photogrammetry and Remote Sensing*, vol. 67, pp. 13 – 26, 2012.